SUPPLEMENTARY INFORMATION

A phase diagram for jammed matter

Chaoming Song, Ping Wang, Hernán A. Makse

Here, we describe the details of the calculations leading to the phase diagram of jammed matter. The main theoretical result is the definition of the volume function based on the Voronoi volume of a particle explained in Section I. Section II describes the isostatic condition that defines the ensemble of jammed matter through the Θ_W function. Section III explains the difference between the geometrical, z, and mechanical, Z, coordination number, which is important to define the canonical partition function. Section IV defines the partition function for the ensemble of jammed states under the isostatic condition, $\mathcal{Q}_{\rm iso}$. Section V explains how to solve the partition function $\mathcal{Q}_{\rm iso}$ which leads to the equations of state (4) and (5), and the phase diagram of Fig. 1. Finally, Section VI explains the numerical studies to test the theoretical predictions.

I. VOLUME FUNCTION

The aim of this section is to delineate the statistical theory for calculating the free volume, W, associated with each particle. First we find an analytical formula for the Voronoi volume of each particle. Then a statistical theory finds that the volume function is related to the coordination number:

$$W(z) = \frac{\kappa}{z} V_g, \tag{6}$$

where $\kappa = 2\sqrt{3}$. This free volume function is then used in the canonical partition function to calculate the phase diagram of jammed states.

A. Microscopic volume function

The definition of a Voronoi cell is a convex polygon whose interior consists of all points closer to a given particle than to any other (see Fig. 5a).

Formally, the volume of the Voronoi cell of particle i can be calculated as (see Fig. 5a):

$$\mathcal{W}_i^{\rm vor} = \oint \int_0^{l_i(\hat{s})} r^{d-1} dr ds = \frac{1}{d} \oint l_i(\hat{s})^d ds, \tag{7}$$

where $l_i(\hat{s})$ is the distance from particle i to the boundary of its Voronoi cell in the $\hat{s}$ direction, and d is the dimension. If one denotes the distance from particle i to any particle j as $\vec{r}_{ij} = r_{ij}\hat{r}_{ij}$ and its projection along the $\hat{s}$ direction as $l_{ij}(\hat{s}) \equiv r_{ij}/(\hat{s}\cdot\hat{r}_{ij})$, then $l_i(\hat{s})$ is the minimum of $l_{ij}(\hat{s})/2$ over all particles j for any $l_{ij}(\hat{s}) > 0$ (see Fig. 5a). This leads to $l_i(\hat{s}) = \min_{l_{ij}(\hat{s})>0} l_{ij}(\hat{s})/2 = \min_{\hat{s}\cdot\hat{r}_{ij}>0} \frac{r_{ij}}{2\hat{s}\cdot\hat{r}_{ij}}$. Substituting into Eq. (7), we find that the volume of the Voronoi cell of particle i is:

$$\mathcal{W}_i^{\rm vor} = \frac{1}{d}\oint \left(\min_{\hat{s}\cdot\hat{r}_{ij}>0} \frac{r_{ij}}{2\hat{s}\cdot\hat{r}_{ij}}\right)^d ds. \tag{8}$$

The geometrical interpretation of this formula is given in Fig. 5a. Equation (8) is relevant in that *(i)* it provides a formula for the Voronoi volume for any dimension in terms of the particle positions or contact network r_{ij}, and *(ii)* it allows for the calculation of macroscopic observables via statistical mechanics. However, further analytical developments are difficult since the volume function of a single particle depends on all particle positions in the system, implying intrinsically strong correlations. Such correlations are implicit in the global minimization of Eq. (8) which, in practice, is restricted to a few coordination shells, defining a mesoscopic Voronoi length scale. Next we present a theory of volume fluctuations to coarse grain $\mathcal{W}_i^{\rm vor}$ over this mesoscopic length scale. The coarsening reduces the degrees of freedom r_{ij} to one variable, the geometrical coordination number z, and defines a mesoscopic volume function amenable to statistical calculations.

Equation (8) can be rewritten as $\mathcal{W}_i^{\rm vor} = \frac{1}{\oint ds}\oint \mathcal{W}_i^s ds = \langle \mathcal{W}_i^s\rangle_s$, where we define the orientational volume for the i particle in the $\hat{s}$ direction as:

$$\mathcal{W}_i^s \equiv V_g \left(\frac{1}{2R}\min_{\hat{s}\cdot\hat{r}_{ij}>0} \frac{r_{ij}}{\hat{s}\cdot\hat{r}_{ij}}\right)^d. \tag{9}$$

The two volumes (8) and (9) are additive and tile the system so that the total system volume is $V = \sum_i \mathcal{W}_i^{\rm vor} = \sum_i \langle \mathcal{W}_i^s\rangle_s$. For isotropic packings, $\mathcal{W}_i^s$ (without the orientational average over $\hat{s}$) is also additive since the choice of orientation $\hat{s}$ is arbitrary. Thus, we obtain:

$$V = \sum_i \langle \mathcal{W}_i^s\rangle_s = \langle \sum_i \mathcal{W}_i^s\rangle_s = \sum_i \mathcal{W}_i^s. \tag{10}$$

This property reduces the number of calculations, since there is no need for an orientational average. The free volume function is defined as

$$W = \mathcal{W} - V_g, \tag{11}$$

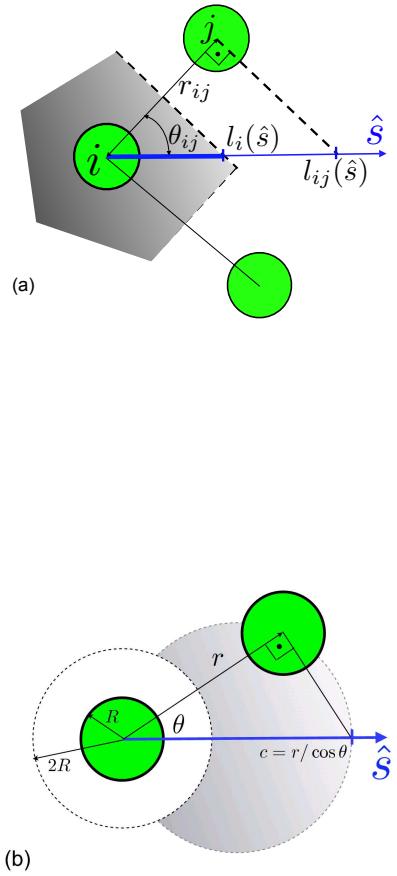

FIG. 5: **Definition of the volume function depicted in 2d for easier visualization**. **a,** The Voronoi volume is the light grey area. The boundary of the Voronoi cell of particle i along the direction $\hat{s}$ is $l_i(\hat{s}) = l_{ij}(\hat{s})/2 = r_{ij}/2\cos\theta_{ij}$, where θ_{ij} is the angle between $\hat{s}$ and r_{ij}. The particle j is said to be closer, along the $\hat{s}$ direction, to i than any other particle. Then the Voronoi volume is proportional to the integration of $l_i(\hat{s})^3$ over $\hat{s}$ as in Eq. (8). **b,** Schematic illustration of the derivation of $P_{\rm B}(c)$. The considered particle (green) is located in the center, the closest particle in the $\hat{s}$ direction is at (r, θ), and the white area is the excluded zone $r < 2R$ for the center of any other grain. For a fixed $c = r/\cos\theta$, the light grey area is the region of the plane (r', θ') where $r'/\cos\theta' < c$. The computation of $P_{\rm B}$ involves the calculation of this volume as explained in the text.

and the reduced free volume function w for isotropic systems is defined as:

$$w \equiv \langle w^s \rangle_i \equiv \left\langle \frac{\mathcal{W}_i^s - V_g}{V_g} \right\rangle_i = \left\langle \left(\frac{1}{2R} \min_{\hat{s}\cdot\hat{r}_{ij}>0} \frac{r_{ij}}{\hat{s}\cdot\hat{r}_{ij}} \right)^d - 1 \right\rangle_i . \tag{12}$$

The isotropic free volume function (12) requires averaging over the particles i but not over $\hat{s}$. The more general form (8) allows study of anisotropic systems, a case left for future work.

B. Mesoscopic volume function

Next, we follow a statistical analysis to find the mesoscopic volume function by averaging the single grain function of Eq. (12). For a given grain i, the calculation of (12) reduces to finding the ball with $\min_j r_j/\cos\theta_j$, where the minimization is over all the grains j (see Fig. 5b for notation, here $r_j = r_{ij}$, $\cos\theta_j = \hat{s}\cdot\hat{r}_{ij}$, and we have set $2R = 1$ for simplicity and we now work in $3d$). We consider that the particle minimizing $r_j/\cos\theta_j$ is located at (r,θ) with $c = r/\cos\theta$ along the $\hat{s}$ direction (see Fig. 5b). We compute the inverse cumulative distribution function $P_>(c)$ to find all the particles j with $r_j/\cos\theta_j > c$. Thus, $P_>(c)$ is the probability that all particles have $r_j/\cos(\theta_j)$ larger than c. The mesoscopic free volume function is then obtained as the mean value $w \equiv \langle w^s \rangle_i = \langle c^3 \rangle - 1$ over the probability density $-\frac{dP_>(c)}{dc}$, and therefore

$$\begin{aligned} w = \langle w^s \rangle_i &= \int_1^\infty (c^3-1)\frac{d[1-P_>(c)]}{dc}dc = -\int_1^\infty (c^3-1)\frac{dP_>(c)}{dc}dc = \\ &= -\int_1^0 (c^3-1)dP_> = \int_0^1 (c^3-1)dP_>. \end{aligned} \tag{13}$$

The integration in Eq. (13) ranges from 1 to ∞ respect to c since the minimum distance for a ball is for $r = 1$ and $\theta = 0$ which gives $c = 1$ and the maximum is at $r \to \infty$. When changing variables to $dP_>$, the limits of integration $c : [1,\infty)$ correspond to the inverse cumulative distribution function $P_> : [1,0]$.

The inverse cumulative distribution function $P_>(c)$ has two contributions: from the contact balls, $P_{\rm C}(c)$, and from the balls in the bulk, $P_{\rm B}(c)$. $P_{\rm C}(c)$ is a surface term that depends on z while $P_{\rm B}(c)$ is the bulk contribution depending on the density of particles. Geometrically, they represent the probabilities for a particle in contact or in the bulk, respectively, to be located outside the light grey area in Fig. 5b, and therefore not contributing

to the volume c^3. The contributions are assumed to be independent of each other, then $P_>(c) = P_{\rm B}(c)P_{\rm C}(c)$.

The background is assumed uniform, with mean free volume density $\rho(w) = N/(NV_g\phi^{-1} - NV_g) = 1/(V_g w)$ and inverse volume fraction $\phi^{-1} = w + 1$, and therefore $P_{\rm B}$ assumes a Boltzmann-like distribution of the form:

$$P_{\rm B}(c) = e^{-\rho(w)V^*(c)}, \tag{14}$$

where $V^*(c) = 2\pi \int_1^\infty \int_0^{\pi/2} \Theta(c - r/\cos\theta) d\vec{r}$ is the volume of the light grey area in Fig. 5b. We obtain:

$$V^*(c) = V_g \left((c^3 - 1) - 3(1 - \frac{1}{c}) \right). \tag{15}$$

Therefore,

$$P_{\rm B}(c) = \exp\left[- \left((c^3 - 1) - 3(1 - 1/c) \right) / w \right]. \tag{16}$$

Similarly, the contact contribution is

$$P_{\rm C}(c) = e^{-\rho_S S^*(c)}, \tag{17}$$

where

$$S^*(c) = 2\pi \int_0^{\arccos(1/c)} \sin\theta d\theta = 2\pi(1 - \frac{1}{c}), \tag{18}$$

and $\rho_S(z)$ is the mean free surface density (the surface analogue of $\rho(w)$).

The contact distribution can be written as $P_C(c) = \exp(-zS^*(c)/S_f)$, where S_f is determined by the mean of $S^*(c)$, $\langle S \rangle$, as $\rho_S(z) \equiv 1/\langle S \rangle = z/S_f$. The exponential distribution is analogous to the background form $P_B(c)$ where we consider $\rho_S(z)$ as the mean free surface density [the surface analogue of $\rho(w)$] representing the inverse of the average area along one direction $\hat{s}$ left free by z contact balls. Formally, S_f is calculated by locating at random z non-overlapping spheres in contact with a given particle. For a given direction $\hat{s}$, the closest particle to $\hat{s}$ defines the angle θ^* from where the free surface is calculated as $S_f = 2\pi(1 - \cos\theta^*)$. In order to estimate the value of S_f, we first calculate the mean of $\cos\theta^*$ for a single particle $z = 1$, which is equal to $S_f = 2\pi$, since $\cos\theta^*$ ranges uniformly from 1 to -1. In the case of many contact particles, $z > 1$, many body constraints imply that the free surface should be corrected by the solid angle extended by a single ball. Thus, up to first order approximation, $S_f \approx 2\pi + S_{\rm occ}$, where $S_{\rm occ} = 2\pi \int_0^{\pi/6} \sin\theta d\theta = 2\pi(1 - \sqrt{3}/2)$ is the surface occupied by a single contact ball. This analysis suggests that the surface term

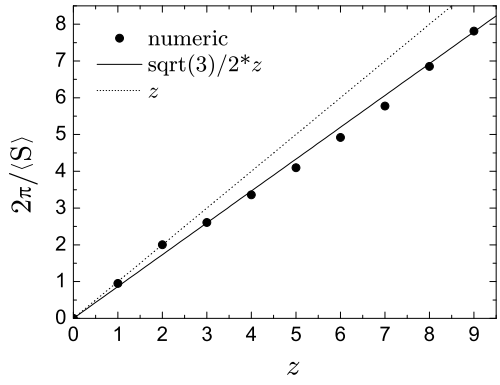

FIG. 6: A numerical calculation of hard spheres confirms that $2\pi\rho_S(z) = \frac{2\pi}{\langle S\rangle}$ is better approximated by $\frac{\sqrt{3}}{2}z$ than z.

can be approximated as $\rho_S(z) \approx z\sqrt{3}/(4\pi)$, a result that is confirmed by computer simulations in Fig. 6. This numerical calculation considers randomly locating z non-overlapping spheres in contact with a given particle. The sphere closest to the direction $\hat{s}$ defines the free angle θ^* and the free surface $S_f = 2\pi(1-\cos\theta^*)$. We find:

$$P_{\rm C}(c) = \exp[-\sqrt{3}z(1-1/c)/2]. \tag{19}$$

The inverse cumulative distribution is then:

$$P_{>}(c) = \exp\left[-\frac{1}{w}\left((c^3-1) - 3(1-\frac{1}{c})\right) - \frac{\sqrt{3}}{2}z(1-\frac{1}{c})\right]. \tag{20}$$

Substituting into Eq. (13), we obtain a self-consistent equation to calculate w:

$$w = \int_0^1 (c^3-1)\ d\exp\left[-\frac{1}{w}\left((c^3-1) - 3(1-\frac{1}{c})\right) - \frac{\sqrt{3}}{2}z(1-\frac{1}{c})\right]. \tag{21}$$

Since $w = \int_0^1 (c^3-1) d\exp[-(c^3-1)/w]$, then Eq. (21) can be solved exactly. We start from the identity: $\int_0^\infty x/w\exp(-x/w)dx = w$,

$$1 = \int_0^1 \frac{1}{w}\left((c^3-1) - \alpha(1-\frac{1}{c})\right) d\exp\left[-\frac{1}{w}\left((c^3-1) - \alpha(1-\frac{1}{c})\right)\right], \tag{22}$$

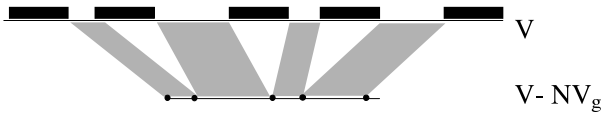

FIG. 7: A mapping between hard sphere and ideal gas in the one dimensional system.

where $\alpha = 3 - wz\sqrt{3}/2$. Or

$$\begin{aligned} 0 &= \int_0^1 \frac{1}{w}(c^3-1)d\exp\left[-\frac{1}{w}\left((c^3-1)-\alpha(1-\frac{1}{c})\right)\right]-1= \\ &= \alpha\int_0^1 \frac{1}{w}\left(1-\frac{1}{c}\right)d\exp\left[-\frac{1}{w}\left((c^3-1)-\alpha(1-\frac{1}{c})\right)\right]. \end{aligned} \tag{23}$$

The second integration in the right hand side is equal to zero only at $w = 0$ or $w \to \infty$, which correspond to two trivial solutions at $\phi = 1$ and $\phi = 0$ respectively. The only non-trivial solution happens at $\alpha = 0$, and therefore $w = 2\sqrt{3}/z$. To see why there are no other solutions, we see that the equation is of the form $\alpha \times I = 0$, where I stands for the second integration. Therefore, all the solutions are for $\alpha = 0$ or $I = 0$. $I = 0$ gives us the two trivial solution and $\alpha = 0$ gives one non-trivial solution, completing the solution space of the original equation. Thus, we arrive at the mesoscopic free volume function which is amenable to analytical calculations:

$$w = \frac{2\sqrt{3}}{z} \quad \Rightarrow \quad W = \frac{2\sqrt{3}}{z}V_g. \tag{24}$$

Equation (24) is a coarse-grained "Hamiltonian" or volume function that replaces the microscopic Eq. (8) in describing the mesoscopic states of jammed matter. While Eq. (8) is difficult to treat analytically, since it requires a field theory, the advantage of the mesoscopic Eq. (24) is that the partition function can be solved analytically since W depends on z only, instead of r_{ij}.

C. Test of the assumptions of the theory.

Below we test the different assumptions of the theory. In 3D, the volume associated with each ball should be greater than the size of the ball. In the case of 1D, a distribution of possible arrangements of hard-spheres corresponds to the distribution of ideal gas particles by removing the volume occupied by the size of the ball (see Fig. 7). Such a mapping is exact in 1D, which implies the exponential distribution in terms of the free volume. To see this, consider a system of volume V (or a system of linear size L in 1D) and a smaller

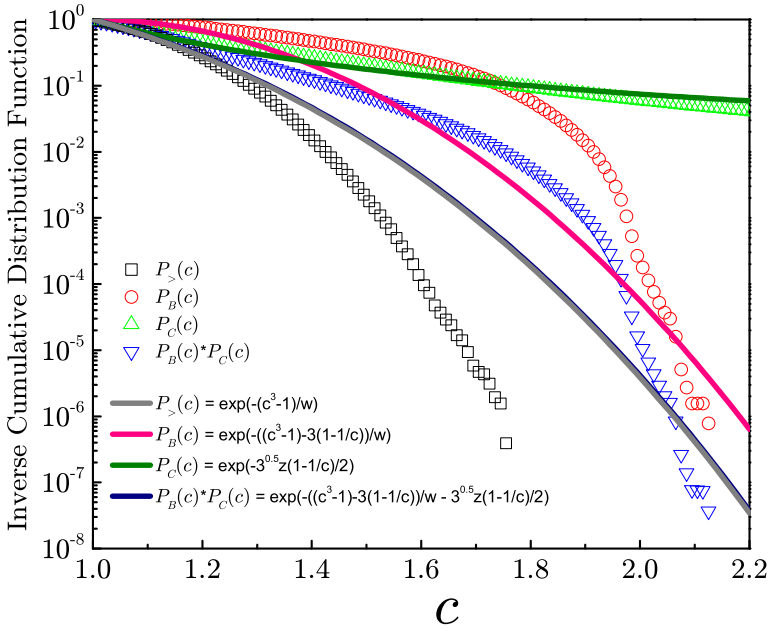

FIG. 8: Comparison between theory and simulations for the inverse cumulative distributions, $P_{\rm B}(c), P_{\rm C}(c)$, $P_{\rm B}(c) \times P_{\rm C}(c)$ and $P_>(c)$ for a packing at the frictionless point with $z = 6$. Similar results are obtained for frictional packings.

part of this volume, V^*. The probability for one particle to be outside the volume V^* is $P(1) = (1 - V^*/V)$. For N independent particles, we obtain $P(N) = (1 - V^*/V)^N$. We set $V^*/V = 1/x$ and the density $\rho = N/V$. Then $P(N) = (1 - 1/x)^{\rho V} = (1 - 1/x)^{\rho x V^*}$. In the limit $x \to \infty$, we obtain a Boltzmann-like distribution: $e^{-\rho V^*}$.

While the above derivation is an exact 1D solution, the extension to higher dimensions is an approximation, since there exists additional geometrical constraints. Even if there is a void with enough volume to be occupied by a particle (that is the volume of the void is larger or equal than the size of the particle), the constraint imposed by the geometrical shape of the particle (which does not exist in 1D) might prevent the void for being occupied. As the simplest approximation we assume the exponential distribution to be valid in 3D.

Next, we test the exponential forms of the cumulative distributions, as well as their correlations, by computer simulations of packings at the frictionless point. The results are plotted in Fig. 8. We first calculate independently $P_{\rm B}(c)$ and $P_{\rm C}(c)$. For a given ball, we choose a direction $\hat{s}$ at random and then find the ball [situated at (r, θ)] with the minimum value of $r/\cos\theta$. More precisely, we find $\min_{\hat{s}\cdot\hat{r}_{ij}>0} \frac{r_{ij}}{2\hat{s}\cdot\hat{r}_{ij}}$, for a fixed direction $\hat{s}$. We then collect data for 400 different directions.

For a given direction, we find two minimum values of c independently as c_b and c_c over all particles in the packing. The c_b is only provided by the ball in the background, and c_c is only provided by the ball in contact. From the probability density, we then calculate the cumulative probability to find a ball at position r and θ such that $r/\cos\theta > c$. That is, we calculate the cumulative distribution of c_b and c_c individually, i.e., $P_{\rm B}(c)$ and $P_{\rm C}(c)$.

The purpose of this calculation is, firstly, to test the predictions of the theory Eq. (16) and (19) for $P_{\rm B}(c)$ and $P_{\rm C}(c)$, and, secondly, to test whether the background distribution is independent of the contact one by comparing $P_{\rm B}(c) \times P_{\rm C}(c)$ with $P_{>}(c)$. The latter is calculated from the simulations by counting all the balls without differentiating between background and contact balls.

The inverse cumulative distributions in Fig. 8 show that the theory approximately captures the trend of these functions but deviations exist as well, especially for large c values. The contact term $P_{\rm C}(c)$ is well approximated by the theory, while the background term shows deviations for larger c; for smaller c the theory is not too far from simulations. We point out that the mesoscopic volume function, w, is extracted from the mean value of $\langle w^s \rangle$ as $w = \langle w^s \rangle = \langle c^3 \rangle - 1$. Indeed, we find that the average $\langle w^s \rangle$ is well reproduced by the theory, and that the deviations from the theoretical probabilities for $w^s > \langle w^s \rangle$ appear not to contribute significantly towards the average volume function. This is seen in the fact that we obtain a good approximation to the volume fraction of the packing even though the full distributions show deviations at larger w^s. For instance, the packing used to obtain the results of Fig. 8 has a volume fraction $\phi = 0.64$ as measured from the particle positions. This value agrees with the average $\langle w^s \rangle$ obtained from the prediction of the probability distribution $P_{>}(c)$. We find $\langle c^3 \rangle = 1.561$, then $\langle w^s \rangle = \langle c^3 \rangle - 1 = 0.561$ and $\phi = 1/\langle c^3 \rangle = 1/(\langle w^s \rangle + 1) = 0.641$ in agreement with the volume fraction of the entire packing obtained from the position of all the balls, 0.64. This shows that the theory approximates well the mean value $\langle w^s \rangle$ (which is needed to obtain accurate estimations of the volume fraction), even though the full distribution presents deviations from the theory. Therefore, the main results of the theory, that is that the Voronoi or quasi-particle volume decreases with the number of contacts, and that the coordination number decreases by increasing friction are not affected by the assumption of the theory.

From Eqs. (20) and (24) we find the distribution of orientational Voronoi volumes. We reproduce the exponential tail in the Voronoi distribution found in experimental studies of

Aste *et al.* [13] and Dauchot *et al.* [14]. We calculate $P(w^s)$ from computer simulations at the frictionless point (details are given in Section VI). The results are shown in Fig. 9 where we see that the theory is able to reproduce the exponential tail in the distribution. However, the distribution from simulations is not a pure exponential but there are corrections at small w^s. We observe that the average value $\langle w^s \rangle$ is well described by the theory. We find $\langle w^s \rangle = 0.561$, which gives a volume fraction $\phi = 1/(1 + \langle w^s \rangle) = 0.641$, in agreement with the direct measurement of the volume fraction of the packing which is 0.64. Thus, the present theory gives a good approximation to the average Voronoi volume needed for the mesoscopic volume function. The theory underestimates the simulations in the range from $w^s \approx 1.5$ to $w^s \approx 2$ and overestimates in the range from $w^s \approx 2$ to $w^s \approx 4$, providing a good estimation of the average while still showing deviations in the full distribution. In order to capture all the moments of the distribution a more refined theory is needed. Such a theory will include the corrections to the exponential forms of $P_{\rm B}(c)$ and $P_{\rm C}(c)$ and their correlations.

The correlations between the contact and bulk term are quantified by comparing $P_{\rm B}(c) \times P_{\rm C}(c)$ with $P_{>}(c)$ in Fig. 8. From the figure we see that below and around the mean $\langle c \rangle$, the full distribution is close to the theoretical result while deviations appear for larger c. Further, a test of the existence of correlations between $P_{\rm B}(c)$ and $P_{\rm C}(c)$ is obtained by calculating the product-moment coefficient of Pearson's correlation as follows.

In the simulation, we pick up a direction $\hat{s}$ randomly, and collect c_b and c_c defined as:

$$c_b = \min_{\hat{s}\cdot\hat{r}_{ij}>0} \frac{r_{ij}}{2\hat{s}\cdot\hat{r}_{ij}}, \quad r_{ij} > 2R, \qquad c_c = \min_{\hat{s}\cdot\hat{r}_{ij}>0} \frac{r_{ij}}{2\hat{s}\cdot\hat{r}_{ij}}, \quad r_{ij} \leq 2R. \tag{25}$$

The Pearson's coefficient is:

$$r^2 = \frac{{S_{bc}}^2}{S_{bb}S_{cc}}, \tag{26}$$

where $S_{bb} = \Sigma({c_b}^2 - \bar{c}_b^2)$, $S_{cc} = \Sigma({c_c}^2 - \bar{c}_c^2)$, and $S_{cb} = \Sigma(c_b c_c - \bar{c}_b \bar{c}_c)$. We find that the Pearson coefficient $r^2 = 0.0173$ is close to zero, meaning that the correlations between $P_B(c)$ and $P_C(c)$ are weak.

The present numerical results imply that the current assumptions of the theory are reasonable. The conclusions are that while the cumulative distributions present deviations from the theory in their tails, the average value of the Voronoi volumes are well captured by the

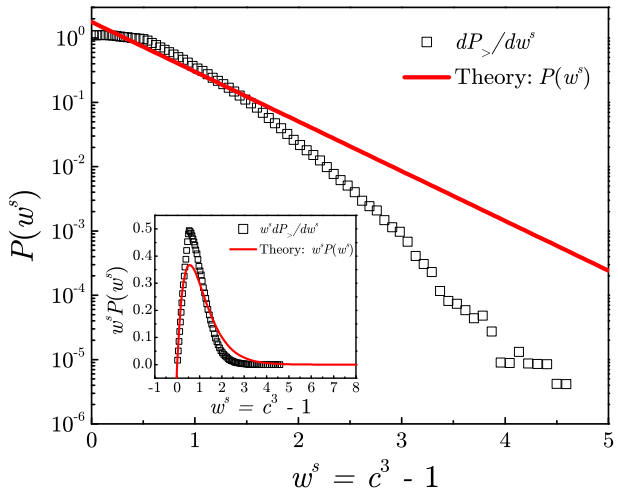

FIG. 9: PDF of w^s. The black squares are simulation results, and the red solid line is the theoretical prediction. The inset plots $w^s P(w^s)$, the integrations of the black square and red solid line give the same value of $\langle w^s \rangle = \phi^{-1} - 1$ despite the observed deviations.

approximations of the theory, which provides, then, an accurate value for the volume function. While the theory considers the full probability distribution of volumes, the w function is defined as the average of this distribution as indicated in Eqs. (13) and (21).

More importantly, the present approach indicates a way to improve the theory to provide more accurate results. Our current studies indicate that we might be able to solve exactly the distribution $P_>(c)$ for a fixed z-ensemble by taking into account the contribution to the volume function from the second coordination shell of particles. Due to the fact that the range of Voronoi cell is finite, it is possible, in principle, to work out a description for the finite, but large, number of degrees of freedom for both disordered and ordered packings through computational linear programming. This approach is related to the Hales' proof of the Kepler conjecture [1]. The present theory is a mean-field version in terms of the restricted description of the disordered packings, which allows us to reduce the dimensionality of the original problem in order to write down the analytic form of the volume function in reasonable agreement with the know values of RCP and RLP. The present approximations of the theory are further supported by the agreement between the obtained form of the volume function and the empirical findings of the experiments of [13].

Below we test the formula Eq. (24) with the well-known example of the FCC lattice at $z = 12$ to assess the approximations in the current version of the theory. At this limiting

number of neighbors the entire class of attainable Voronoi cells have volumes in a narrow range around 0.7 Vg which is significantly larger than the prediction from Eq. (24). The current theory is developed under the assumption of isotropic packings. Isotropic packings are explicitly taken into account in the theory when we consider the orientational Voronoi volume $\mathcal{W}_i^s$ (along a direction $\hat{s}$) as a simplification of the full Voronoi volume, $\mathcal{W}_i^{\rm vor}$. Such a simplification is equivalent to $\mathcal{W}_i^{\rm vor}$ at the mean-field level and meaningful for isotropic packings but fails for anisotropic or ordered packings. The extension of the current theory to anisotropic packings, such as the FCC lattice at $z = 12$, can be carried out, but remains outside of the scope of the present work. In this case, the full Voronoi volume Eq. (8) needs to be used. In fact, it is possible to describe the finite number of degrees of freedom for ordered packings, which is related to the Hales' proof of the Kepler conjecture [1], through computational linear programming.

II. ISOSTATIC CONDITION

Here we explain the usual constraint arguments leading to the existence of the minimal mechanical coordination number at the isostatic point [19–23]. We consider a set of spherical particles interacting via normal and tangential contact forces. These can be the standard Hertz and Mindlin/Coulomb forces of contact mechanics, respectively, see Section VI A. We set N: number of particles, N_n: number of unknown normal forces, N_t: number of unknown tangential forces, E_f: number of force balance equations, E_t: number of torque balance equations, d: dimension, $Z = 2M/N$: average coordination number of the packing, where M is the total number of contacts, $f_1(\mu)$: undetermined function of the friction coefficient μ such that $1-f_1(\mu)$ is the fraction of spheres that can rotate freely ($f_1(0) = 0$ and $f_1(\infty) = 1$), and $f_2(\mu)$: undetermined function of μ indicating the ratio of contacts satisfying $F_t < \mu F_n$, where F_n, and F_t are the normal and tangential forces respectively at the contact, which satisfies $f_2(0) = 0$ and $f_2(\infty) = 1$.

A packing is isostatic when the number of contact forces equal the number of force and torque balance equations, i.e.:

$$N_n + N_t = E_f + E_t. \tag{27}$$

TABLE I: Number of constraints and variables determining the isostatic condition for different systems.

Friction	N_n	N_t	E_f	E_t
$\mu = 0$	$\frac{1}{2}NZ$	0	dN	0
μ finite	$\frac{1}{2}NZ$	$\frac{1}{2}(d-1)NZf_2(\mu)$	dN	$\frac{1}{2}d(d-1)Nf_1(\mu)$
$\mu = \infty$	$\frac{1}{2}NZ$	$\frac{1}{2}(d-1)NZ$	dN	$\frac{1}{2}d(d-1)N$

The average coordination number at the isostatic point is then (see Table I):

$$Z(\mu) = 2d\frac{1 + 1/2(d-1)f_1(\mu)}{1 + (d-1)f_2(\mu)}, \tag{28}$$

reducing to the known $Z = 2d$ for frictionless particles and $Z = d + 1$ for infinitely rough particles. The relation $Z(\mu)$ is an important assumption of the theory. Figure 10 shows $Z(\mu)$ obtained in simulations for different preparation protocols explained in Section VI. It should be noted that other protocols could give rise to other dependence of Z on μ. However, since the phase diagram is given in terms of Z, the main prediction of Fig. 1 would still be valid.

Another way to see the equation $Z(\mu)$ is the following. For finite μ, we have to consider additional Coulomb conditions. The calculation of $Z(\mu)$ becomes a nonlinear problem except when $\mu \to 0$ and $\mu \to \infty$. The problem can be understood as an optimization of an outcome based on a set of constraints, i.e., minimizing a Hamiltonian of a system over a convex polyhedron specified by linear and non-negativity constraints. Equation (27) can be augmented to indicate the number of extra equations for contacts satisfying the Coulomb condition, which is analogous to the number of redundant constraints in Maxwell constraint counting of rigidity percolation. This suggests that, for a finite value of μ, the original nonlinear problem can be mapped to a linear equation problem if we know how many extra equations should be added.

III. GEOMETRICAL AND MECHANICAL COORDINATION NUMBER

The derivation of the volume function in Section I implies nothing about the value of the contact forces; the volume function represents the contribution arising purely from the

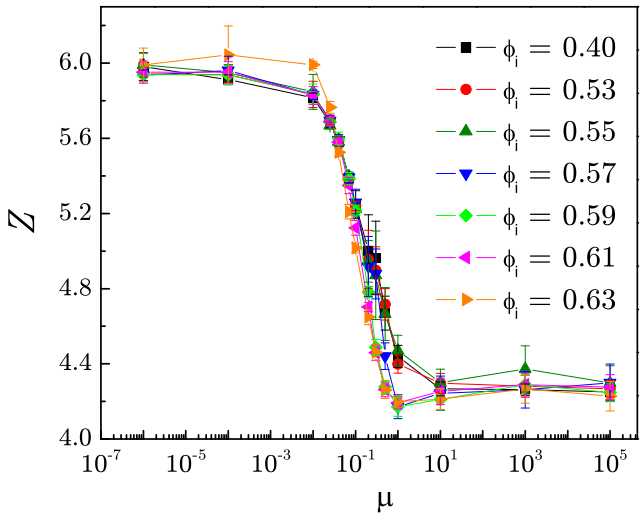

FIG. 10: Mechanical coordination number versus friction μ obtained in our numerical simulations explained in Section VI for different preparation protocols characterized by the initial volume fractions ϕ_i indicated in the figure. The symbols and parameters used in these simulations are the same as in the plot of Fig. 4.

geometry of the packing. Thus, the coordination number z appearing in Eq. (1) is the *geometrical* coordination number related to volume, which is different from the *mechanical* coordination number Z that can be measured through the force contact network relating to the isostatic condition. In general we expect $Z \leq z$, since some geometrical contacts may carry no force. To show this, imagine a packing of infinitely rough ($\mu \to \infty$) spheres with volume fraction close to 0.64. There must be $z = 6$ nearest neighbors around each particle on the average. However, the mechanical balance law requires only $Z = 4$ contacts per particle on average, implying that 2 contacts have zero force and do not contribute to the contact force network.

Such a situation is possible: starting with the contact network of an isostatic packing of frictionless spheres having $z = 6$ and all contacts carrying forces (then $Z = 6$ also), we simply allow the existence of tangential forces between the particles and solve the force and torque balance equations again for this modified system of infinitely rough spheres. Such a solution is guaranteed to exist due to the isostatic condition. The resulting packing is mechanically stable and is obtained by setting to zero the forces of two contacts per ball, on

average, to satisfy the new force and torque balance condition for the additional tangential force at the contacts. Despite mechanical equilibrium, giving $Z = 4$, there are still $z = 6$ geometrical contacts contributing to the volume function. Therefore, we identify two types of coordination number: the geometrical coordination number, z, contributing to the volume function and the mechanical coordination number, Z, measuring the contacts that carry forces only.

These ideas are corroborated by numerical simulations in Section VI and explained in Section III A, below. The packings along the vertical RCP line found in the simulations (see Fig. 4 in the main text) have approximately the same geometrical coordination number, $z \approx 6$. However, they differ in mechanical coordination number, going from the frictionless point $Z = 6$ to $Z \approx 4$ as the friction coefficient is increased (see Section VI C).

A. Bounds of the geometrical coordination number, z.

We have proposed in the main text that the bounds of the geometrical coordination number are $Z \leq z \leq 6$ imposed by the isostatic condition. Below we test these bounds with computer simulations (for technical details of the computer simulations we refer to Section VI). The interpretation of z considers it as a coarse-grained average associated with "quasiparticles" with free volume W. The reason to use a coarse grained measure to define the coordination number is in the quasiparticle character of the theory. The calculation of the W function implies a coarse graining over a distance which is found to be of the order of two beads diameters; below we find numerically that the 'quasiparticles" size is of the order of two particle diameters. Once z is averaged over this range, we find that z is ranging approximately between $(Z, 6)$. Thus the theory considers the mesoscopic fluctuations associated with each quasi-particle. In the limiting case of no mesoscopic fluctuations, when $X = 0$ along the RCP line, we find a very narrow distribution at $z = 6$ for any value of Z and μ, after averaging z over a mesoscopic region of two particle diameters. The distribution is even narrower when z is coarse-grained over a region of four particle diameters.

Thus, the bounds $(Z, 6)$ are shown to hold under reasonable accuracy; well approximated by the assumption in the theory. The X-ray tomography experiments of Aste [13] (Fig. 6a) reveal the trend predicted by Eq. (1) between the inverse of the Voronoi volume and the average number of neighbors of a set of Voronoi cells with similar volumes. However, it is

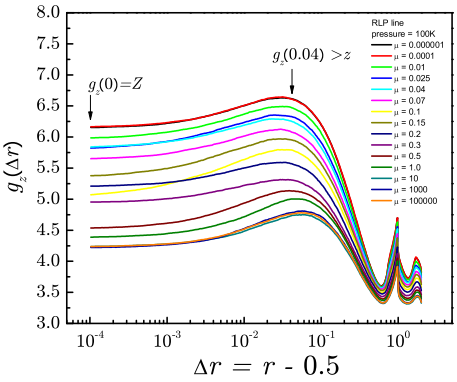

FIG. 11: $g_z(\Delta r)$ of packings with various friction coefficient μ along RLP line.

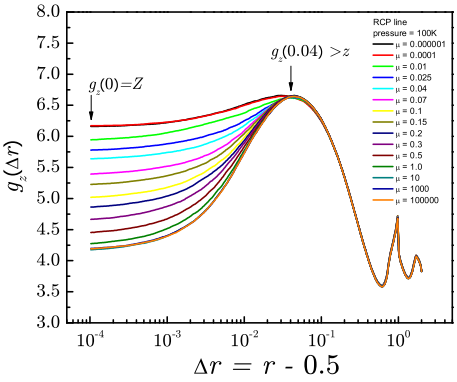

FIG. 12: $g_z(\Delta r)$ of packings with various friction coefficient μ along RCP line.

evident from the figure that such average number of neighbors is spanning a range of values between ~ 4 and ~ 10. The reason why the Aste's group found wider range of z is possibly due to the fact they did not consider such a range of coarse-graining.

In order to identify the geometrical coordination number, z, and the mechanical coordination number, Z, we define a modified radial distribution function $g_z(r)$ as:

$$g_z(r) = \frac{1}{N}\frac{R^2}{r^2}\sum_{i}^{N}\sum_{j\neq i}^{N}\Theta(\frac{r_{ij}}{r-R})\Theta(\frac{r+R}{r_{ij}}), \quad r > R \tag{29}$$

where R is the radius of particle, N is the number of particles, r_{ij} is the distance of two particle's centers, $r_{ij} = |\vec{r}_i - \vec{r}_j|$, and Θ is the Heaviside step function. $g_z(r)$ describes the average value of the number of grains in contact with a virtual particle of radius r, and the factor of R^2/r^2 is the ratio of a real sphere's area and the virtual one's. Figures 11 and 12 plot the $g_z(\Delta r)$ of packings with various friction coefficient μ on the isostatic plane along the RLP and RCP lines respectively, where we define $\Delta r = \frac{r-R}{2R}$ (noticed that in the figures,

we set $2R = 1$ for simplicity). Following the definition of Eq. (29), g_z with $\Delta r = 0$ should be directly equal to the mechanical coordination number, Z, and should range from 4 to 6 along both RLP and RCP lines which is confirmed by our numerical simulations in Fig. 11 for the RLP line and Fig. 12 for the RCP line.

Furthermore, as shown in the figures, we find that $g_z(\Delta r)$ along the RCP line, increases slightly as Δr increases, and finally reach the same value of g_z at $\Delta r = 0.04$ as shown in Fig. 12, indicating that all RCP states have approximately the same geometrical coordination number, $z \sim 6$. This is in agreement with the theoretical bounds. We notice that $g_z(\Delta r = 0.04) = 6.65 > 6$, which results from the increasing of the coordination number at the critical point as the local volume fraction ϕ increases slightly as $Z - Z_c \sim (\phi - \phi_c)^\beta$.

Furthermore, we study the coarse-grained coordination number $\langle z \rangle_l$ as defined as,

$$\langle z \rangle_l = \frac{1}{N_l} \frac{R^2}{r^2} \sum_{i}^{N_l} \sum_{j \neq i}^{N_l} \Theta(\frac{r_{ij}}{r - R}) \Theta(\frac{r + R}{r_{ij}}), \quad r > R \tag{30}$$

where N_l is the number of the particles inside a coarse-grained spherical range with a radius of l. Fig. 13 and Fig. 14 plot the PDF of $\langle z \rangle_l$ for all the packings along the RLP and RCP lines respectively. The distributions show a Gaussian shape, and the average value gives the value of $g_z(r)$, i.e.,

$$\overline{\langle z \rangle_l} = g_z(r). \tag{31}$$

We find that all the $P(\langle z \rangle_l)$ along RCP line coincide at $\Delta r = 0.04$ as shown in Fig. 14b and 14c, demonstrating that all the states have approximately the same average value (as it should be since the RCP line is at $X = 0$), but also the distribution of the geometrical coordination number. The distribution gets narrower as the coarse-graining parameter l increase from $l = 2$ to $l = 4$ as shown in Fig. 14c. This demonstrate that the bounds proposed by the theory are satisfied for the RCP line.

Along the RLP line, the situation is analogous. Since this line corresponds to $X \to \infty$ we should expect different average z as we move along the line varying the friction coefficient. This is clearly demonstrated in Fig. 13b which should be compared with the analogous Fig. 14b for the RCP line. More importantly, we find that the bounds of $\langle z \rangle_l$ are well approximated between the bounds given by the isostatic condition $(4, 6)$ in agreement with the assumptions of the theory. The slight shift towards higher coordinations observed in Fig.

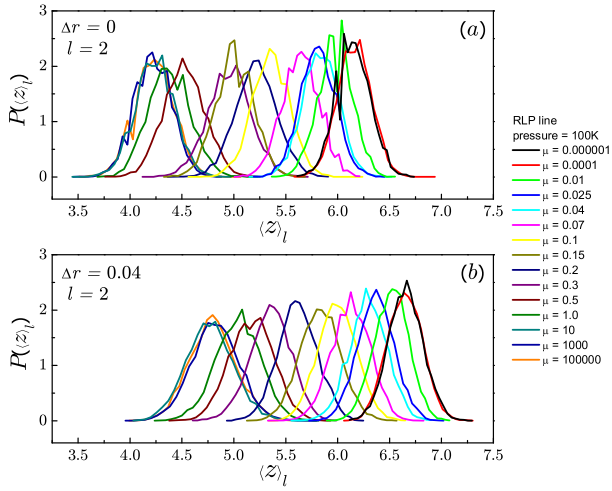

FIG. 13: PDF of the coarse-grained coordination number $\langle z \rangle_l$ for packings with various friction coefficient μ along the RLP line. (a) $\Delta r = 0$ and $l = 2$; (b) $\Delta r = 0.04$ and $l = 2$.

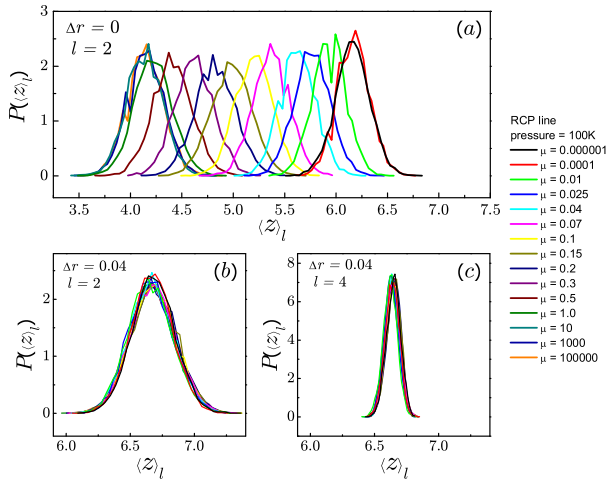

FIG. 14: PDF of the coarse-grained coordination number $\langle z \rangle_l$ for packings with various friction coefficient μ along the RCP line. (a) $\Delta r = 0$ and $l = 2$; (b) $\Delta r = 0.04$ and $l = 2$; (c) $\Delta r = 0.04$ and $l = 4$.

13b is due to the small increment in volume fraction from the critical point of jamming, as discussed above. Overall, we conclude that the bounds assumed by the theory are a good approximation.

IV. PARTITION FUNCTION

According to the statistical mechanics of jammed matter proposed by Edwards [7], the volume partition function $\mathcal{Q}$ is defined as:

$$\mathcal{Q} = \int g(W) e^{-W/X} \Theta_W dW, \tag{32}$$

where W is the free volume function, X is the compactivity measured in units of volume, $g(W)$ is the density of states for a given volume W, and Θ_W imposes the condition of jamming.

Since W is directly related to the geometrical coordination number z through Eq. (6), $g(W)$ is computed by changing variables,

$$g(W) = \int P(W|z) g(z) dz, \tag{33}$$

where $P(W|z)$ is the conditional probability of a free volume W for a given z, and $g(z)$ is the density of states for a given z.

Here, z is the geometrical coordination number related with volume, different from the mechanical one, Z. From the arguments explained in Section III, z must be larger than or equal than the mechanical coordination number Z and bounded by the maximum coordination number for a random packing, which is $2d = 6$. That is,

$$g(W) = \int_Z^6 P(W|z) g(z) dz. \tag{34}$$

The density of states $g(z)$ can be understood in three step. First, we consider that the packing of hard spheres is in a jammed configuration in which there can be no collective motion of any contacting subset of particles that leads to unjamming. This definition corresponds to the collectively jammed category proposed by Torquato and co-workers [24]. It is a sensible definition of jammed configurations since it goes beyond the merely locally jammed configuration of packings that are unstable to the motion of a single particle. While the degrees of freedom are continuous, the fact that the packing is collectively jammed implies that the jammed configurations in the volume space are not continuous. Otherwise there would be a continuous transformation in the position space that would unjam the system contradicting the fact that the packing is collectively jammed. Thus, we consider that the configuration space of jammed matter is discrete since we cannot change one configuration to another in a continuous way.

Second, we call the dimension per particle of the configuration space as $\mathcal{D}$ and consider that the distance between two jammed configurations is not broadly distributed (meaning that the average distance is well-defined). We call the mean distance between configurations in the volume space as h_z, and therefore the number of configuration is proportional to $1/(h_z)^{\mathcal{D}}$.

Third, we add z constraints per particle due to the fact that the particle is jammed by z contacts. Thus, there are Nz position constrains ($|\vec{x}_i - \vec{x}_j| = 2R$, where $\vec{x}_i$ is the position of the particle i) for a jammed state of hard spheres as compared to the unjammed "gas" state. Therefore, the number of degrees of freedom is reduced to $\mathcal{D} - z$, and the number of configurations is then $1/(h_z)^{\mathcal{D}-z}$. Since the term $1/(h_z)^{\mathcal{D}}$ is a constant, it will not influence the partition function. Therefore, we obtain $g(z) = (h_z)^z$.

The situation is analogous to the discreteness of the configuration space imposed by the Heisenberg principle in quantum mechanics. While the degrees of freedom $\{p_i, q_i\}$ are continuous, the uncertainty principle imposes the discreteness $\Delta p \Delta q \sim h$. In equilibrium statistical mechanics the dimension per particle of the configuration space is d, and a density of states is obtained as $1/h^d$.

The conditional probability $P(W|z)$ depends on the W function, $W = \frac{2\sqrt{3}}{z} V_g$. The average is taken over a certain mesoscopic length scale since the volume of a particle depends on the positions of the particles surrounding it. Practically, such length scale is approximately of several particle diameters. W is a coarse-grained volume and independent of the microscopic partition of the particles, implying:

$$P(W|z) = \delta(W - \kappa/z). \tag{35}$$

Substituting Eq. (35) and Eq. (34) into Eq. (32), we find the isostatic partition function used in Eq. (3) in the main text (we set $V_g = 1$ for simplicity, i.e. we measure the compactivity in units of V_g):

$$\mathcal{Q}_{\rm iso}(X, Z) = \int_Z^6 (h_z)^z \exp\left(-\frac{2\sqrt{3}}{zX}\right) dz. \tag{36}$$

V. CALCULATION OF THE EQUATIONS OF STATE.

Here we provide details of the calculations leading to the equations of state (4) and (5). From the partition function (36), we calculate the average volume fraction $\phi^{-1} = W/V_g + 1 = 2\sqrt{3}/z + 1 = (2\sqrt{3} + z)/z$ as:

$$\phi(X, Z) = \frac{1}{\mathcal{Q}_{\rm iso}(X, Z)} \int_Z^6 \frac{z}{z + 2\sqrt{3}} \exp\left(-\frac{2\sqrt{3}}{zX} + z \ln h_z\right) dz, \tag{37}$$

where $(h_z)^z = \exp[z \ln h_z]$, note that $\ln h_z < 0$, since $h_z \ll 1$. In the limit of $X \to 0$, only the minimum volume or ground state at $z = 6$ contributes to the partition function. Then Eq. (37) gives Eq. (4):

$$\phi_{\rm RCP} = \phi(X = 0, Z) = \frac{6}{6 + 2\sqrt{3}} \approx 0.634, \quad Z(\mu) \in [4, 6], \tag{38}$$

plotted in Fig. 1 as the RCP line.

When $X \to \infty$, $\exp(-2\sqrt{3}/(zX)) \to 1$, and the average in (37) is over all states with equal probability:

$$\phi_{\rm RLP}(Z) = \phi(X \to \infty, Z) = \frac{1}{\mathcal{Q}_{\rm iso}(\infty, Z)} \int_Z^6 \frac{z}{z + 2\sqrt{3}} \exp\left(z \ln h_z\right) dz. \tag{39}$$

The constant h_z determines the minimum volume in the phase space and therefore $h_z \ll 1$. Then the leading contribution to Eq. (39) is from the highest volume at $z = Z$ and therefore:

$$\phi_{\rm RLP}(Z) \approx \frac{Z}{Z + 2\sqrt{3}}, \quad Z(\mu) \in [4, 6], \tag{40}$$

plotted in Fig. 1 as the RLP line. For finite X, Eq. (37) can be solved numerically. For each X, the function $\phi(X, Z)$ can be obtained and is plotted as each isocompactivity color line in Fig. 1. Finally, the entropy can also be calculated as

$$S(X, Z) = \langle W \rangle / X + \ln \mathcal{Q}_{\rm iso}(X, Z) \tag{41}$$

This equation is obtained in analogy with equilibrium statistical mechanics and it is analogous to the definition of free energy: $F = E - TS$ where $F = -T \ln \mathcal{Q}$ is the free energy, T is the temperature and E the average energy. We replace $T \to X$, $E \to \langle W \rangle$. Therefore, $F = E - TS$ or $S = (E - F)/T = E/T + \ln \mathcal{Q}$ is now $S(X, Z) = \langle W \rangle / X + \ln \mathcal{Q}_{\rm iso}(X, Z)$, which is plotted as the equation of state in Fig. 3. For the calculation of S we consider

$g(z) = {h_z}^{z-2d}$ since for $z = 2d$ there is only one mesoscopic state or $g(z) = e^{-\frac{z-2d}{z_c}}$ with $z_c = \frac{1}{\ln(h_z^{-1})} = 0.01$ as used in Fig. 3 and 4. This correction is irrelevant for average quantities like $\phi(X, Z)$ but important for the entropy.

VI. SIMULATIONS

A. Molecular dynamics simulations of grains

We prepare static packings of spherical grains interacting via elastic forces and Coulomb friction. The system size ranges from $N = 1,024$ to $N = 10,000$ particles. In the microscopic model, two spherical grains in contact at positions $\vec{x}_1$ and $\vec{x}_2$ and with radius R interact with a Hertz normal repulsive force

$$F_n = \frac{2}{3}\, k_n R^{1/2} \delta^{3/2}, \tag{42}$$

and an incremental Mindlin tangential force

$$\Delta F_t = k_t (R\delta)^{1/2} \Delta s, \tag{43}$$

(see [21] for more details). Here the normal overlap is $\delta = (1/2)[2R - |\vec{x}_1 - \vec{x}_2|] > 0$. The normal force acts only in compression, $F_n = 0$ when $\delta < 0$. The variable s is defined such that the relative shear displacement between the two grain centers is $2s$. The prefactors $k_n = 4G/(1-\nu)$ and $k_t = 8G/(2-\nu)$ are defined in terms of the shear modulus G and the Poisson's ratio ν of the material from which the grains are made. Typically, $G = 29$ GPa and $\nu = 0.2$ for spherical glass beads and we use $R = 5 \times 10^{-3}$ m and the density of the particles, $\rho = 2 \times 10^3$ kg/m^3. Viscous dissipative forces are added at the global level affecting the total velocity of each particle through a term $-\gamma \dot{\vec{x}}$ in the equation of motion, where γ is the damping coefficient related to the viscosity of the medium $\eta = \gamma/(6\pi R)$. Sliding friction is also considered:

$$F_t \leq \mu F_n. \tag{44}$$

That is, when F_t exceeds the Coulomb threshold, μF_n, the grains slide and $F_t = \mu F_n$, where μ is the static friction coefficient between the spheres. We measure the time in units of $t_0 = R\sqrt{\rho/G}$, the compression rate in units of $\Gamma_0 = 5.9 t_0^{-1}$ and the viscosity in units of $\eta_0 = 8.2 R^2 \rho / t_0$.

B. Preparation protocols: Packings at the jamming transition

The preparation protocol consists of first preparing a gas of non-interacting particles at an initial volume fraction ϕ_i in a periodically repeated cubic box. The particles do not interact and therefore the stress in the system is $\sigma = 0$ and $Z = 0$. To achieve any particular volume fraction in this initial stage, we apply an isotropic compression without friction. The final results do not depend on the details of this preparation since the system is still below the jamming condition, retaining the characteristics of a fluid. After obtaining this state with initial volume fraction ϕ_i, a compression is applied with a compression rate Γ until a given volume fraction ϕ_1. Then the compression is stopped and the system is allowed to relax to mechanical equilibrium by following Newton's equations for translations and rotations without further compression.

This protocol can generate packings with different volume fractions. Simulations reveal that there is a critical volume fraction at the jamming transition ϕ_c, below which a jammed packing with nonzero pressure can not be obtained. After the compression with Γ, two things can occur:

(a) The system jams: If the system is above the jamming point $\phi_1 > \phi_c$, then the stress will decrease and ultimately stabilize to a finite nonzero value, meaning that the pressure of the system remains unchanged (usually $\Delta\sigma < 10^{-3}$ Pa) over a large period of time (usually $\sim 10^7$ MD steps). The coordination number usually has a first initial decrease, but if the system is jammed it will also stabilize at a constant value above the isostatic minimal number.

(b) The system is not jammed: here the stress and the coordination number will relax to zero. If the packing has $\phi_1 > \phi_c$, it stabilizes at a non-zero pressure above the jamming transition, but the pressure decreases very fast to zero (the system is not jammed) if $\phi_2 < \phi_c$, even though ϕ_1 and ϕ_2 may differ only by 2×10^{-4}.

In order to identify the exact volume fraction of the jamming transition, we apply a split algorithm to find ϕ_c as follows [27]. A search procedure consisting of several cycles is applied such that in each cycle we fix the lower and upper boundaries of ϕ_c. The difference between the boundaries gets smaller as the cycles proceed, meaning that ϕ_c is fixed with higher and higher precision. We start from the packing of high volume fraction $\phi_1 > \phi_c$ and generate a series of packings with step-decreasing volume fractions until the first packing

with zero pressure is observed, which has a volume fraction $\phi = \phi_1 - \Delta\phi$. Thus, ϕ_c is bounded between $\phi_1 - \Delta\phi$ and ϕ_1. Then we test $\phi = \phi_1 - \Delta\phi/2$. If $\phi = \phi_1 - \Delta\phi/2$ is stable, ϕ_c is between $\phi_1 - \Delta\phi$ and $\phi_1 - \Delta\phi/2$. If $\phi = \phi_1 - \Delta\phi/2$ is unstable, ϕ_c is between $\phi_1 - \Delta\phi/2$ and ϕ_1. Therefore, in this cycle, we reduce the region where ϕ_c possibly lies in from $\Delta\phi$ to $\Delta\phi/2$. If we carry out this cycle for n times, we improve the precision to $\Delta\phi_n = \Delta\phi/2^n$. In our simulations cycling ceases when $\Delta\phi_n$ gets below 2×10^{-4} and $n = 12$. A similar algorithm was employed in [27] to study the approach to the jamming transition by preparing packings at a finite pressure. In the present work we are interested in jammed packings at vanishing pressure, right at the jamming transition in the isostatic plane defined for all friction coefficients.

This algorithm obtains packings at the critical density of the jamming transition with high precision, $\phi_c \pm 2 \times 10^{-4}$ (notice that in the main text we denote $\phi_c = \phi$ for simplicity). In Fig. 4 we simulate jammed packings by starting with configurations with ϕ_i and performing the split algorithm to find ϕ_c. We repeat this procedure 10 times with different random initial configurations to get a better average of ϕ_c. Each data point in Fig. 4 corresponds to a single set of $(\phi_i, \Gamma, \eta, \mu)$ and is averaged over these 10 realizations. We consider $0.40 \leq \phi_i \leq 0.63$, $10^{-7} \leq \Gamma \leq 10^{-3}$, $10^{-4} \leq \eta \leq 10^{-3}$, and $0 \leq \mu \leq \infty$. The error of ϕ_c obtained over the 10 realizations as shown in Fig. 4 is usually 5×10^{-4}, larger than the precision of the split algorithm (2×10^{-4}).

It is important to determine whether the packings are jammed in the sense that they are not only mechanically stable but also they are stable under perturbations. Our numerical protocols assure that the system is at least locally jammed since each particle is in mechanical equilibrium [24]. To test if the system is collectively jammed is more involved. For frictionless systems, where tangential forces are removed, we use the Hertz energy $U_{\rm hertz} = \frac{4}{15}\, k_n R^{1/2} \delta^{5/2}$ to test whether the Hessian of the jammed configurations is positive [22]. We find that the frictionless configurations have positive Hessian indicating that they are collectively jammed. However, this method is not useful when considering frictional systems. The energy of deformation depends on the path taken to deform the system and cannot be defined uniquely. In this case, a numerical test of the stability of the packings applies a small random velocity to each jammed particle. We find that the packings are stable to small perturbations consisting of external forces of the order of 0.1 times the value of the average force, indicating that the packings may be collectively jammed.

To test for more strict jammed conditions involves studying the stability under boundary deformations. We have tested that our packings are stable under the most common strain deformations to isotropic packings by performing a uniaxial compression test, a simple shear and a pure shear test.

For instance, a simple shear test implies a strain deformation $\Delta\epsilon_{12} = \Delta\epsilon_{21} \neq 0$, while the rest of the strain components ϵ_{ij} remain constant. A pure shear test is done with $\Delta\epsilon_{11} = -\Delta\epsilon_{22} \neq 0$ and a uniaxial compression test along the 1-direction is performed by keeping the strain constant in $\Delta\epsilon_{22} = \Delta\epsilon_{33} = 0$, and $\Delta\epsilon_{11} \neq 0$. Here, the strain ϵ_{ij}, is determined from the imposed dimensions of the unit cell. For example, $\epsilon_{11} = \Delta L/L_0$ where ΔL is the infinitesimal change in the 11 direction and L_0 is the size of the reference state.

In all cases the packings are stable under strain perturbations. A full investigation of the elasticity of the jamming phase diagram is left for future studies. It suffices to state that the numerically found states can be considered to be mechanically stable jammed states.

C. Results

Knowledge of the existence of the packings in the phase diagram opens such predictions to numerical and experimental investigation. Next, we test the theoretical predictions and show how to dynamically generate all the packings in the phase space of configurations through different preparation protocols. In particular we provide a scheme to reproduce the RCP and RLP-lines amenable to experimental tests. We parameterize the preparation protocol by the initial volume fraction ϕ_i, the compression rate Γ, and the dissipative properties of the medium where the particles are disperse, the viscosity η. The system is defined by the friction coefficient μ.

In Fig. 4 we plot the final state ϕ against the mechanical coordination number of the packings Z for different preparation protocols parameterized by $(\phi_i, \Gamma, \eta, \mu)$.

The main plot in Fig. 4 explores the dependence of the packings (ϕ, Z) on the initial state ϕ_i. We plot our results for a fixed quench rate $\Gamma = 10^{-7}$ and damping coefficient $\eta = 10^{-3}$ (except for the last orange curve on the right with $\eta = 10^{-4}$) and for different initial states ranging from left to right (see Fig. 4 for details) $\phi_i = 0.40$ (black ■), 0.53 (red •), 0.55 (violet ▲), 0.57 (blue ▼), 0.59 (green ♦), 0.61 (pink ◄) and 0.63 (orange ►). Each data point corresponds to a prepared system at a given friction from $\mu = 0$ at $Z \approx 6$ to $\mu \to \infty$

at $Z \approx 4$.

We find that the packings prepared from the larger initial densities ϕ_i closely reproduce the RCP line of zero compactivity at $\phi_{\rm RCP}$. Therefore RCP exists not only at the frictionless J-point at $Z = 6$ but extend along the vertical line until $Z \approx 4$. This corroborates one of the predictions of the theory that RCP states can be found for any value of friction coefficient, not just for frictionless packings. We conclude that RCP is not confined to a single point in the phase diagram but corresponds to the many states along the RCP line.

We find that the packings along the RCP-line have equal geometrical coordination number $z \approx 6$ but differ in their mechanical one from $Z = 6$ to $Z \approx 4$, in agreement with theory. These states are then identified with the ground state of jammed matter as depicted in the volume landscape picture of Fig. 2a.

In the limit of small densities for the initial state (see curves for $\phi_i = 0.40, 0.53, 0.55$ in the phase space Fig. 4), we reproduce approximately the predictions of the RLP-line. These packings follow the theoretical prediction for infinite compactivity except for small (less than 5%) deviations in the coordination number for packings close to the lower value of $Z = 4$. We find the lowest possible volume fraction at $\phi_{\rm RLP}^{\rm min} = 0.539 \pm 0.003$, close to the theoretical prediction, $\phi_{\rm RLP}^{\rm min} = 0.536$, which approximately agrees with the lowest stable volume fraction ever reported experimentally by Onoda and Liniger, $\phi_{\rm RLP}^{\rm min} = 0.550 \pm 0.006$ for monodisperse hard spheres [5].

Packings with the lowest Z correspond to infinitely rough spheres. The deviation of coordination number between theory and simulation (specially at low volume fraction) could be from the system not achieving an isostatic state at infinite friction. In general, we find that while there are many states along the RLP line, the barriers of these states decrease as the coordination number decreases towards $Z = 4$, i.e. when the friction increases. Thus, the states at the lower left part of the phase diagram are the most difficult to equilibrate.

Besides the states delimiting the phase space, we generate other packings with intermediate values of $\phi_i = 0.57, 0.59, 0.61$ as shown in Fig. 4. Interestingly, we find that these states (all obtained for fixed $\Gamma = 10^{-7}$ and $\eta = 10^{-3}$) closely follow the predicted lines of isocompactivity as indicated in the figure. We find that the simulations from $\phi_i = 0.57, 0.59, 0.61$ correspond to compactivities $X = 1.62, 1.38$, and 1.16, respectively (measured in units of $10^{-3}V_g$). The constant h_z weakly affects the finite compactivity states. We find that $h_z = 0.01$ provides the best fit to the data for finite isocompactivity lines in Fig. 4. Other

values of h_z produce approximately the same phase diagram boundaries (i.e., the RLP and RCP lines, as long as $h_z \ll 1$) but with different isocompactivity lines within.

At this point we do not have a theoretical explanation for why packings with the same initial state ϕ_i have the same compactivity. We may conjecture that ϕ_i determines a type of disorder quenched in the initial configuration that leads to systems with the same compactivity but different volume fractions and coordination numbers, evidenced by our results. We can use this empirical result to control the compactivity of the packing, at least for this particular protocol. Laboratory measurements of compactivity usually involve indirect measures through fluctuation-dissipation relations between fluctuations and response functions [8, 11, 30]. Our results can be used to, at a minimum, define packings with equal compactivity. The empirical identification of X with ϕ_i promotes the possibility of controlling X within this particular protocol.

We also test the dependence on the state of the packings with the compression rate Γ and viscosity η. Both parameters should have similar effects since they slow down the dynamics of the grains. In general, we reproduce the RLP line for slow quenches or for large viscosities as seen in the inset of Fig. 4. In this case, the grains are allowed to slide and develop large transversal displacements and Mindlin forces with the concomitant low ϕ and large compactivity. Therefore we find a predominance of the Mindlin forces over the normal Herztian forces as a characteristic of the lower volume fractions of RLP, having large compactivity in the packing. When the compression rate is increased or the damping is reduced we find packings with higher volume fractions as indicated in the inset of Fig. 4.